Interaction of sine-Gordon kinks with defects: phase space transport in a two-mode model

Roy H. Goodman [a,b,1], Philip J. Holmes [b,c,*], Michael I. Weinstein [a]

[a] *Mathematical Sciences Research, Bell Laboratories—Lucent Technologies, Murray Hill, NJ 07974, USA*
[b] *Program in Applied and Computational Mathematics, Princeton University, Princeton, NJ 08544, USA*
[c] *Department of Mechanical and Aerospace Engineering, Program in Applied and Computational Mathematics, Department of Mechanical and Aerospace Engineering, Princeton University, Princeton, NJ 08544, USA*

Abstract

We study a model derived by Fei et al. [Phys. Rev. A 45 (1992) 6019] of a kink solution to the sine-Gordon equation interacting with an impurity mode. The model is a two degree of freedom Hamiltonian system. We investigate this model using the tools of dynamical systems, and show that it exhibits a variety of interesting behaviors including transverse heteroclinic orbits to degenerate equilibria at infinity, chaotic dynamics, and an extremely complex and delicate structure describing the interaction of the kink with the defect. We interpret this in terms of phase space transport theory. © 2002 Elsevier Science B.V. All rights reserved.

1. Introduction and motivation

There has been much recent interest in the propagation of nonlinear waves through variable or noisy media. Perhaps the simplest problem to study is the interaction of a nonlinear wave with a localized defect in an otherwise homogeneous medium. Such a defect may do many things to a traveling wave. It may speed the wave up, slow it down, or break it apart altogether. In a particular application, we have performed numerical studies [14] showing the possibility of trapping light by the introduction of specially engineered defects into optical fiber waveguides with periodic structure (Bragg grating fibers). Nonlinear propagation in such structures is described by the nonlinear coupled mode equations (NLCME) [9,15], which possess a family of traveling wave solutions known as *gap solitons*. This trapping may be modeled as the interaction of a such a gap soliton with bound states arising due to the localized defect.

Several studies have been undertaken to try to understand these soliton–defect interactions. The first approach is numerical experimentation using direct simulation of the initial value problem for the evolution equations. In our

---

* Corresponding author.
E-mail address: pholmes@rimbaud.princeton.edu (P.J. Holmes).
[1] Present address: Department of Mathematical Sciences, New Jersey Institute of Technology, University Heights, Newark, NJ 07102, USA.
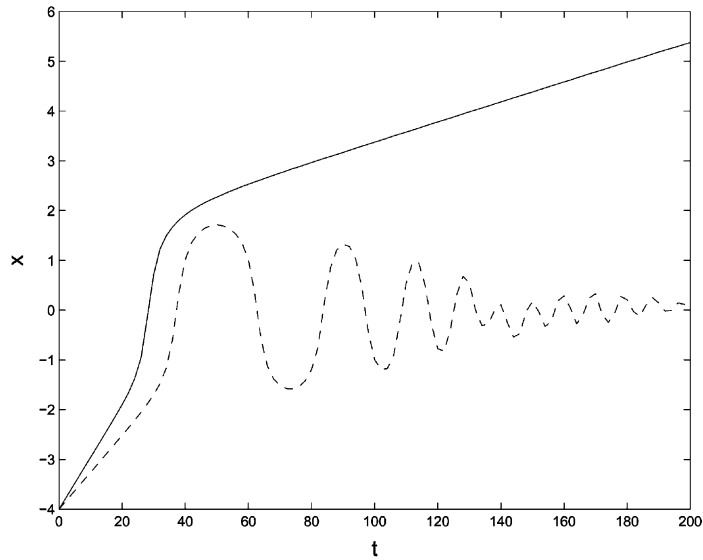
Fig. 1. Space–time tracks of the peaks of gap solitons that are captured and transmitted by a defect.

experiments for the NLCME, we found a rich variety of behaviors. In all experiments, a gap soliton was initialized propagating toward the defect with no energy in the defect mode. We found different scenarios resulting from the interaction: trapping, reflection, transmission, or some combination thereof. Similar behavior was observed by Cao and Malomed [7] in numerical studies of nonlinear Schrödinger solitons.

Fig. 1 shows the paths, in the space–time plane, of the peaks of two gap solitons exhibiting transmission and capture. We observed that, in the case of trapping, the energy of the trapped mode slowly decayed, presumably due to nonlinear coupling to radiation modes [29]. The scenario that occurs depends on details of the incoming soliton (velocity, amplitude and phase) as well as the defect shape: see [14].

A second approach is to derive finite dimensional models which reproduce the essential dynamics of the soliton–defect interaction. One way to do this is to approximate the solution by a superposition of a small set of 'modes', characterized by time-dependent parameters (collective coordinates), and then use these parameters to form a reduced *effective* Lagrangian for the system. Evolution equations are then derived as the Euler–Lagrange equations for the effective Lagrangian. This procedure is explained in more depth in Section 2. Such models have been derived for the sine-Gordon and ϕ^4 equations by Fei and coworkers [10,11,19], and by Forinash et al. for the nonlinear Schrödinger equation [12]. The resulting models are finite systems of ordinary differential equations or differential–algebraic equations. The model derived in [11] for the sine-Gordon equation is a two degree of freedom Hamiltonian system and it is this system we investigate here, as a prototype of the more complex, higher dimensional system corresponding to the NLCME. We are able to provide a rather complete analytic description of the behavior of this system.

In [23], equations governing the dynamics of kink and breather locations are derived by a direct perturbation procedure. In cases where the full system derives from a Lagrangian, this approach gives similar finite dimensional collective coordinate equations to those obtained from the effective Lagrangian approach. However, this procedure is also applicable when the full equations are not Lagrangian. Moreover, this framework enables one to systematically study the problem of the accuracy of the reduction, see also [30,32]. The study of [23] is done for a general class of defects perturbing the sine-Gordon equation with dissipative and driving terms. It emphasizes the effects of dissipation and driving on the dynamics of coherent structures, and in some cases "pinning" of kinks was found: a phenomenon similar to capture studied here.

Fei et al. [11] note three possible behaviors for a kink solution of the sine-Gordon equation interacting with a defect. Above a critical velocity, the kink passes through the defect, albeit with diminished speed. Below this critical speed, they find that the kink is captured, except in certain "resonance bands" where the kink "interacts a finite number of times with the defect" before returning in the direction from which it came. Our phase space analysis of the finite dimensional ODE reduction, yields a concise picture of what it means for the kink to "interact a finite number of times with the defect". Fei et al. use the finite dimensional reduction derived from an effective Lagrangian to give a heuristic derivation of the critical velocity for the PDE, with good agreement.

On the other hand, our simulations and analysis of this reduction indicate a strong contrast between the reduced dynamics and the infinite dimensional dynamics of the PDE. While for the finite dimensional reduction, we find capture for finite times, in all cases, the kink eventually escapes from the defect and moves off at reduced constant speed, leaving some of its energy in the defect mode. In addition to being reflected back toward its starting position, the kink can also be transmitted and continue traveling in the original direction. Applying methods of dynamical systems analysis, we show that the system of ordinary differential equations has very complicated dynamics, which can be understood by examining the stable and unstable manifolds of a fixed point at infinity for an associated *Poincaré map*. We show that the initial conditions leading to reflection and transmission by the defect are intricately interwoven, essentially forming the gaps separating points in a zero-measure Cantor set of initial conditions of orbits that are trapped for all time. Thus, the finite dimensional reduced system displays sensitive dependence to initial conditions. Closer qualitative agreement with the PDE dynamics is obtained by inclusion of an appropriate damping term in the reduced system, reflecting the mechanism of radiation damping. Thus, a finite dimensional Lagrangian description does not succeed in capturing important features of the long-time dynamics, but it may be improved by inclusion of an effective damping, an infinite dimensional effect due to coupling of the kink–defect subsystem with the radiative "heat bath".

This paper is organized as follows. In Section 2, we review the two-mode model of Fei et al. and in Section 3, we briefly describe their results. The central Section 4 contains an analysis of the model via the methods of dynamical systems theory. Using Hamiltonian reduction and introducing a (small) parameter, we show that a Poincaré map defined on a suitable cross section of each constant energy manifold can be approximated, and prove that the stable and unstable manifolds of distinguished points at infinity intersect transversely. Phase space transport methods then allow us to (partially) characterize sets of initial conditions for kinks that are transmitted without capture, captured and eventually transmitted or reflected, and captured for all time. We provide numerical illustrations of these behaviors in Section 5. In Section 6, we discuss the role played by coupling to radiation modes, an effect present in the full infinite dimensional PDE, and modify the two-mode model accordingly. Finally, in Section 7, we summarize and draw conclusions.

2. The model

Following Fei et al. [11], we consider a sine-Gordon model with a localized impurity at the origin:

$$u_{tt} - u_{xx} + \sin u = \epsilon \delta(x) \sin u. \tag{2.1}$$

In the absence of any impurity, i.e. $\epsilon = 0$, the sine-Gordon equation has the well-known family of kink solutions parameterized by speed V:

$$u_{\mathrm{k}}(x, t) = 4 \tan^{-1} \exp \left(\frac{x - Vt - x_0}{\sqrt{1 - V^2}} \right). \tag{2.2}$$

If we consider the system with an impurity, then solutions of small amplitude approximately satisfy the linear equation

$$u_{tt} - u_{xx} + u = \epsilon \delta(x) u,\tag{2.3}$$

which, for $0 < \epsilon < 2$, has standing wave solutions

$$u_{\text{im}}(x, t) = a(t) \, e^{-\epsilon|x|/2},\tag{2.4}$$

where $a(t) = a_0 \cos(\Omega t + \theta_0)$ and

$$\Omega = \sqrt{1 - \tfrac{1}{4}\epsilon^2}.\tag{2.5}$$

Fei et al. [11] study the interaction of the kink and defect modes using a collective coordinate approach to derive a set of approximate equations for the evolution of the kink position X, and the defect mode amplitude a. To derive the approximate equations, they substitute the ansatz

$$u = u_{\text{k}} + u_{\text{im}} = 4 \tan^{-1} \exp(x - X(t)) + a(t) \, e^{-\epsilon|x|/2}\tag{2.6}$$

into the Lagrangian of Eq. (2.1)

$$L = \int_{-\infty}^{\infty} \left(\tfrac{1}{2} u_t^2 - \tfrac{1}{2} u_x^2 - [1 - \epsilon \delta(x)](1 - \cos u) \right) \, dx.\tag{2.7}$$

Here, X replaces $x_0 + Vt$, and a and X, the parameters characterizing the approximate solution Eq. (2.6), are regarded as unknown functions of t. It is assumed that a and ϵ are small enough that many cross-terms can be neglected. Thus, in calculating the effective Lagrangian, all terms produced via overlap of the two-modes are neglected, excepting those which include the defect potential $\delta(x)$. This is equivalent to assuming that the dominant means of interaction between the two-modes is via the defect. All terms that are neglected under this assumption contain oscillatory integrals which should average out to be much smaller than the terms retained. Evaluating the spatial integrals of Eq. (2.7), an effective Lagrangian $L_{\text{eff}}(X, a, \dot{X}, \dot{a})$ is obtained [11]:

$$L_{\text{eff}} = 4\dot{X}^2 + \frac{1}{\epsilon}(\dot{a}^2 - \Omega^2 a^2) - U(X) - aF(X),\tag{2.8}$$

where

$$U(X) = -2\epsilon \operatorname{sech}^2(X),\tag{2.9}$$

$$F(X) = -2\epsilon \tanh(X) \operatorname{sech}(X).\tag{2.10}$$

The corresponding evolution equations are then given by the classical Euler–Lagrange equations for Eq. (2.8):

$$8\ddot{X} + U'(X) + aF'(X) = 0;\tag{2.11a}$$

$$\ddot{a} + \Omega^2 a + \frac{\epsilon}{2} F(X) = 0.\tag{2.11b}$$

This system corresponds to a particle X moving in an attractive potential well $U(X)$ which is exponentially localized in a neighborhood of zero, coupled to a harmonic oscillator a by an exponentially localized term $aF(X)$. Note that this model inherits many properties from the sine-Gordon system. When X is large, $U(X)$ and $F(X)$ are small, so that $\ddot{X} \approx 0$ and the kink may propagate at any constant speed, independent of the impurity mode a, which oscillates at its characteristic frequency Ω. When X becomes small, the two equations become coupled and the kink may exchange energy with the impurity mode.
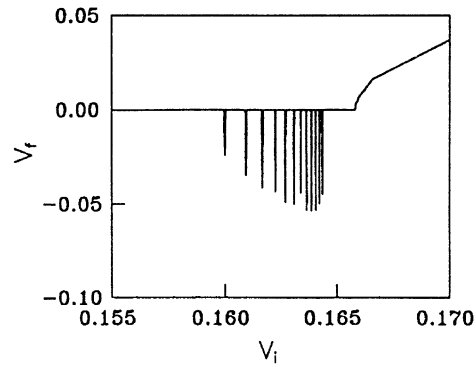
Fig. 2. Capture, reflection and transmission of kinks for the sine-Gordon equation with a defect potential, Eq. (2.1). V_f and V_i denote final and initial kink velocities. From [11], Fig. 9.

3. A heuristic trapping argument

In their numerical studies, Fei et al. [11] initialize the sine-Gordon Eq. (2.1) with a kink solution localized far from the impurity and headed toward it, with zero energy in the impurity mode. They then watch how the kink interacts with the impurity. The basic result of these experiments is that, above a certain critical velocity, the kink passes through the impurity, albeit with diminished speed, having transferred some of its energy to the impurity mode. Below the critical velocity, two possible behaviors emerge. For most values of the initial velocity, the kink is trapped, but there exists a sequence of *resonant* velocities. These mark the centers of narrow bands of initial velocities for which the kink interacts with the impurity mode a finite number of times before being reflected back toward its initial position. Fei et al. [11] do not report any cases of interactions followed by transmission: indeed, transmission behavior was rarely observed [18]. Fig. 2 shows these phenomena in a plot of final versus initial kink velocity.

In related studies of kink–antikink interactions in modified sine-Gordon, ϕ^4 and double sine-Gordon equations, Campbell and coworkers [4–6,25] found similar transmission and reflection phenomena, obtaining final versus initial velocity data similar to that of Fig. 2, as well as phenomenological theory predicting the positions of the resonance windows.

Using Eqs. (2.11a) and (2.11b), an approximate condition for kink trapping is derived based on a one-way exchange of energy from the kink to the impurity mode. Fei et al. further derive a heuristic resonance condition which they use to predict the locations of the first ten or so resonant velocities.

We have performed numerical experiments on Eqs. (2.11a) and (2.11b) and have found some discrepancies with the findings of [11], sketched in the previous section. We initialize $X = -6$, a good distance away from the potential, and $\dot{X} > 0$, with $a = \dot{a} = 0$. We then plot the final velocity of the kink as a function of the initial velocity, see Fig. 3. Note that for the PDE (Fig. 2), there is a critical velocity $v_c = 0.166$, very similar to our value $v_c = 0.169$ for the ODE, above which the kink passes the impurity without any interaction. For velocities below critical, however, any kink which starts sufficiently far from the impurity eventually escapes if we follow the evolution long enough. Additionally, we find that kinks that interact with the defect may leave in either direction: they may be reflected as described above, but they also may be transmitted after interacting with the impurity mode one or more times. This contrasts with Fig. 2 from [11], in which kinks with subcritical initial velocity are captured unless the velocity lies in certain reflection windows, with no evidence of transmission windows. There was rare evidence of transmission for subcritical velocities [18]. Fei et al. suggest a semiheuristic formula for predicting the resonant velocities of the reflection windows, and their formula could easily be adapted to predict the transmission windows as well.
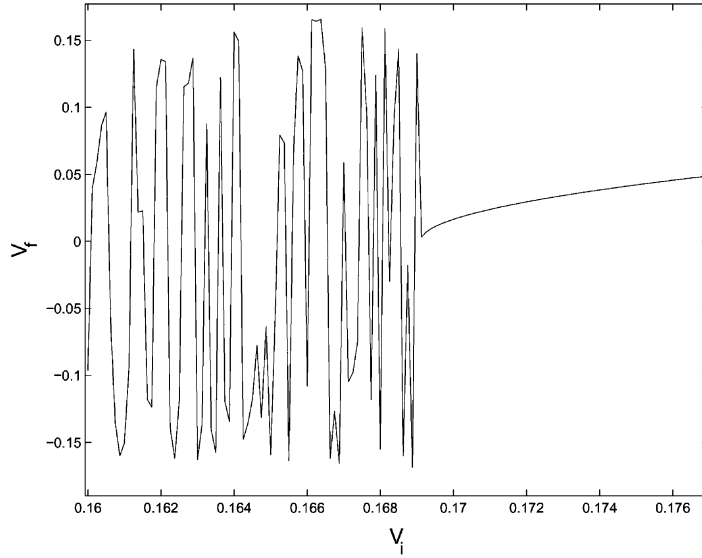
Fig. 3. Capture, reflection and transmission of sine-Gordon kinks for the two-mode ODE model Eqs. (2.11a) and (2.11b) of [11] with $\epsilon = 0.5$. V_f and V_i denote final and initial kink velocities. Compare with Fig. 2.

Our simulations of Eqs. (2.11a) and (2.11b) do not show any trapping for all time, and indeed, through study of Eqs. (2.11a) and (2.11b) as a dynamical system, we show that the set of initial conditions that lead to trapping is nonempty but of measure zero.

4. Dynamical systems analysis

We modify Eqs. (2.11a) and (2.11b) by inserting a coupling parameter $0 \leq \mu \leq 1$ in order to facilitate our analysis:

$$8\ddot{X} + U'(X) + \mu a F'(X) = 0, \tag{4.1a}$$

$$\ddot{a} + \Omega^2 a + \tfrac{1}{2}\epsilon\mu F(X) = 0. \tag{4.1b}$$

We will perform perturbation theory for small μ and also consider the limiting case $\mu = 1$ of Eqs. (2.11a) and (2.11b). It will be convenient to rewrite Eqs. (4.1a) and (4.1b) in Hamiltonian form with momentum variables

$$p_X = \frac{\partial L_{\text{eff}}}{\partial \dot{X}} = 8\dot{X}, \qquad p_a = \frac{\partial L_{\text{eff}}}{\partial \dot{a}} = \frac{2}{\epsilon}\dot{a}, \tag{4.2}$$

and Hamiltonian $H \equiv \dot{X}p_X + \dot{a}p_a - L_{\text{eff}}$:

$$H = \frac{1}{16}p_X^2 + \frac{\epsilon}{4}p_a^2 + \frac{\Omega^2}{\epsilon}a^2 + U(X) + \mu a F(X). \tag{4.3}$$

4.1. Preliminary analysis: symmetries, fixed points, and invariant manifolds

Letting

$$Y = \dot{X} \quad \text{and} \quad b = \dot{a}, \tag{4.4}$$

we find that the system of equations (4.1a) and (4.1b) is invariant under the following symmetries:

$$(X, Y, a, b, t) \rightarrow (-X, -Y, -a, -b, t), \tag{4.5a}$$

$$(X, Y, a, b, t) \rightarrow (-X, Y, -a, b, -t), \tag{4.5b}$$

and $(X, Y, a, b, t) \rightarrow (X, -Y, a, -b, -t)$. (4.5c)

When $\mu = 0$, the X and a dynamics are uncoupled and the Hamiltonian system is completely integrable:

$$H = \frac{1}{16} p_X^2 + U(X) + \frac{\epsilon}{4} p_a^2 + \frac{\Omega^2}{\epsilon} a^2 \stackrel{\text{def}}{=} H^X + H^a \tag{4.6}$$

since the two components of H may be treated separately. The impurity mode a simply oscillates harmonically as

$$a = a_0 \cos \Omega(t - t_0),$$

and the behavior of the kink may be inferred from the phase plane corresponding to H^X, level sets of which are shown in Fig. 4. If $H^X < 0$, the kink position, X, undergoes bounded periodic motion. If $H^X > 0$, it propagates monotonically, approaching a constant velocity for large $|X|$. Between these behaviors there exists a separatrix consisting of a pair of homoclinic orbits to infinity, given by

$$p_X^0 = \pm 4\sqrt{2\epsilon} \operatorname{sech} X^0, \tag{4.7}$$

for which $|X|$ approaches infinity for large times, but with vanishing velocity. The explicit solution along these orbits ($8\dot{X} = \pm 4\sqrt{2\epsilon} \operatorname{sech} X$) is given by

$$X^0 = \pm \sinh^{-1} \sqrt{\tfrac{1}{2}\epsilon}(t - t_1). \tag{4.8}$$

These separatrices are analogous to the parabolic orbits in the Newtonian two-body problem that separate regions of elliptic (periodic) and hyperbolic (unbounded) motions. This geometrical picture is made clear in Fig. 4. Trajectories between the two dotted separatrices represent clockwise motion on closed curves. Solutions above this region move monotonically to the right and those below, to the left. This divides the phase plane into three regions, which we label R_1, R_2, and R_3, starting at the top and going down.

In the uncoupled system, trapping is impossible, since a kink starting from infinity with nonzero velocity necessarily remains outside the (invariant) separatrix and thus will pass through the defect and recover its initial velocity.
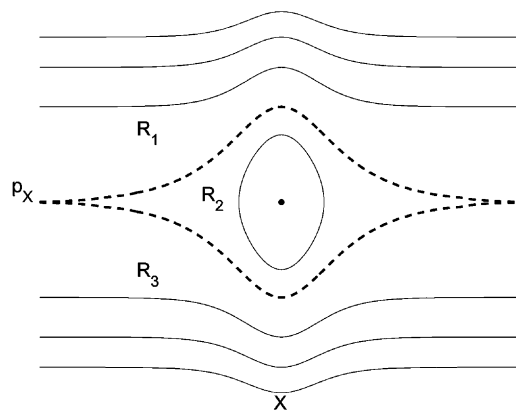

Fig. 4. The phase plane for H^X, the uncoupled X system.

Similarly, solutions starting in R_2 must remain inside the separatrix. Once coupling is added, this may change. By interacting with the oscillator mode when $\mu \neq 0$, the kink can cross between the regions R_1 and R_2 or R_2 and R_3. A kink will be said to interact with the defect if it starts in region R_1 or R_3 and subsequently enters R_2, and to be trapped or captured if it stays in R_2 for all future times.

We will examine the system perturbatively, in the limit of small μ. When $\mu = 0$, the system has one fixed point, a center at the origin. This fixed point persists for μ nonzero. When ϵ is also small, the origin remains an elliptic fixed point, but at

$$\epsilon = \frac{2}{\sqrt{1 + 2\mu^2}},$$

the system undergoes a Hamiltonian pitchfork bifurcation. The origin becomes a saddle-center with one-dimensional stable and unstable manifolds and two new elliptic fixed points appear at

$$X = \pm\operatorname{sech}^{-1}\Psi, \qquad p_X = 0, \tag{4.9}$$

$$a = \frac{\mu\epsilon^2}{\Omega^2} \tanh X \operatorname{sech} X, \qquad p_a = 0, \tag{4.10}$$

where $\Psi = \sqrt{4 + 2\mu\epsilon^2 - \epsilon^2}/2\mu\epsilon$. We will concentrate on the case $\epsilon < 2/\sqrt{1 + 2\mu^2}$ so that the system possesses only one elliptic fixed point.

When $\mu \neq 0$ and the system becomes coupled, the flow can no longer be explained in terms of a two-dimensional phase portrait as in Fig. 4. The system now evolves in the 'full' four-dimensional phase space. However, key features of the uncoupled system remain. For large X, $F(X)$ approaches zero exponentially, so the system is essentially uncoupled. At $X = \pm\infty$, the system has a family of periodic orbits $a = a_0 \cos \Omega(t - t_0)$ which persist for nonzero μ. The 'parabolic' orbits of the uncoupled system are the invariant manifolds of these periodic orbits, which form heteroclinic orbits connecting the fixed points at $X = \pm\infty$. We first show that these stable and unstable manifolds persist when $\mu > 0$, and then show that they in fact continue to intersect, albeit now transversally, so that a structure survives akin to that shown in Fig. 4.

To study the stable and unstable manifolds of the periodic orbits at $|X| = \infty$, we make a change of variables for positive X (one proceeds analogously for $X = -\infty$). Letting

$$q = \operatorname{sech} X, \qquad p = \dot{X},$$

the differential equations become

$$\dot{q} = -qp\sqrt{1 - q^2}, \qquad \dot{p} = -\tfrac{1}{2}\epsilon q^2\sqrt{1 - q^2} - \tfrac{1}{4}\mu\epsilon a q(1 - 2q^2), \tag{4.11}$$

$$\dot{a} = b, \qquad \dot{b} = -\Omega^2 a + \mu\epsilon^2 q\sqrt{1 - q^2}. \tag{4.12}$$

and the periodic orbits are moved to the origin in the (q, p)-plane, where they are contained in a line of degenerate fixed points with $q = 0$ (note that for $\mu = 0$ the linearized vector field in this plane is $Df(0) = 0$). This situation is analogous to the restricted three-body problems treated by McGehee [22], and we may apply his stable manifold theorem for degenerate fixed points of planar maps to the Poincaré return map induced by Eqs. (4.11) and (4.12) on the (q, p)-plane (cf. [8]). For completeness, we state this result in the Appendix A.

By placing the variables a and p_a in action-angle variables (see Section 4.2), we may define a Poincaré map for p and q with respect to the angle θ. This is valid as long as $\partial_t \theta > 0$, which is true for large X (small q), and globally

in the phase space for small μ, as discussed in Section 4.2. Integration of Eq. (4.11) shows that the return map takes the form:

$$
f = \begin{cases} q \mapsto q - K_1 q(p + r_1(q, p)), \\ p \mapsto p - K_2 q(q + r_2(q, p)), \end{cases}
\tag{4.13}
$$

where $r_j(q, p)$ contain higher order terms and K_j denotes a constant. Letting $q = \xi - \eta$, $p = \xi + \eta$, f becomes

$$
f = \begin{cases} \xi \mapsto \xi + p_1(\xi, \eta) + \cdots, \\ \eta \mapsto \eta + p_2(\xi, \eta) + \cdots, \end{cases}
\tag{4.14}
$$

where $p_1 = -K_3(\xi - \eta)\xi$ and $p_2 = K_4(\xi - \eta)\eta$. Thus $p_1(\xi, 0) = -K_3\xi^2 < 0$, $p_2(\xi, 0) = 0$ and $\partial p_2/\partial \eta(\xi, 0) = K_4\xi > 0$ for $\xi > 0$, the hypotheses of McGehee's theorem are satisfied, and we may conclude that analytic stable and unstable manifolds exist. We note that Birnir [2,3] used the McGehee result in his study of rational pole solutions of a periodically forced KdV equation.

4.2. Reduction, Poincaré maps and homoclinic points

The variable a and its conjugate may be expressed in action-angle coordinates [13] I and θ defined by

$$
a = \sqrt{\frac{I\epsilon}{\Omega}} \cos \theta; \qquad p_a = 2\sqrt{\frac{\Omega I}{\epsilon}} \sin \theta,
\tag{4.15}
$$

so that

$$
H^a = \Omega I.
\tag{4.16}
$$

Then the Hamiltonian of the full system becomes

$$
H(X, p_X, I, \theta) = H^X(X, p_X) + \Omega I + \mu H^1(X, p_X, I, \theta),
\tag{4.17}
$$

where

$$
H^1 = \sqrt{\frac{I\epsilon}{\Omega}} \cos \theta F(X).
\tag{4.18}
$$

Hamilton's equations are thus:

$$
\dot{X} = \frac{\partial H}{\partial p_X} = \frac{p_X}{8},
\tag{4.19a}
$$

$$
\dot{p}_X = -\frac{\partial H}{\partial X} = -U'(X) - \mu\sqrt{\frac{I\epsilon}{\Omega}} \cos \theta F'(X),
\tag{4.19b}
$$

$$
\dot{I} = -\frac{\partial H}{\partial \theta} = \mu\sqrt{\frac{I\epsilon}{\Omega}} \sin \theta F(X),
\tag{4.19c}
$$

$$
\dot{\theta} = \frac{\partial H}{\partial I} = \Omega + \frac{\mu}{2}\sqrt{\frac{\epsilon}{\Omega I}} \cos \theta F(X).
\tag{4.19d}
$$

The uncoupled ($\mu = 0$) equations have a family of orbits

$$
I(t) = I^0, \qquad \theta(t) = \Omega t + \theta^0
$$

with X and p_X given in Eqs. (4.7) and (4.8). These correspond to trajectories in the four-dimensional phase space homoclinic to periodic orbits.

Since the Hamiltonian is conserved, the flow is constrained to lie on the invariant three-dimensional energy manifold determined by the initial data:

$$H(X, p_X, I, \theta) = h_0 = \text{constant.} \tag{4.20}$$

For μ sufficiently small, we may invert Eqs. (4.7) and (4.20) to obtain

$$I = I(X, p_X, \theta; h_0) = \frac{1}{\Omega}(h_0 - H^X + \text{O}(\mu)). \tag{4.21}$$

This reduces the system from four dimensions to three, since we need not solve the evolution equation for I. Indeed, as described in Section 4.8 of [16], using the fact that

$$\dot{\theta} = \frac{\partial H}{\partial I} = \Omega + \text{O}(\mu) > 0$$

and eliminating time in favor of the time-like variable θ, we may write the reduced equations on each constant energy manifold $H = h_0$ as a periodically forced single degree of freedom system with Hamiltonian $-I(X, p_X, \theta; h_0)$:

$$X' = -\frac{\partial I}{\partial p_X}, \qquad p'_X = \frac{\partial I}{\partial X}, \tag{4.22}$$

where $(\cdot)'$ denotes $\mathrm{d}/\mathrm{d}\theta(\cdot)$. Note that this implies that Eq. (4.22) preserves phase space volumes on each energy manifold, and hence that the Poincaré maps defined below preserve area.

For $\mu = 0$, Eq. (4.22) is an autonomous planar system whose phase portrait coincides with that of the uncoupled X system of Fig. 4, since in this case, I is simply a scaled version of H^X. However, the 'fixed point' at infinity is really a periodic orbit γ, since, provided that the energy $h_0 > 0$, the I-mode is oscillating ($\theta' = 1$). For $\mu > 0$, Eq. (4.22) becomes nonautonomous, and one may no longer draw phase portraits on the (X, p_X)-plane, but one can define a Poincaré map P_{θ_0} on the cross-section $\Sigma_{\theta_0} = \{(X, p_X; \theta = \theta_0)\}$ [16]. By the theorem of McGehee [22] noted above, γ and its stable and unstable manifolds $W^s(\gamma)$, $W^u(\gamma)$ persist for small μ; indeed, we may compute explicitly that γ is given by $a = (\sqrt{h_0\epsilon}/\Omega)\cos\Omega(t - t_1)$.

In order to show that $W^s(\gamma)$ intersects $W^u(\gamma)$ transversely, we apply Melnikov's method [24] to P_{θ_0}, the Poincaré map generated by following the flow from $\theta = \theta_0$ to $\theta = \theta_0 + 2\pi$. Melnikov's method is generally applied to systems with hyperbolic fixed points in order to find the intersection of the stable and unstable manifolds. For such systems, solutions lying on the stable and unstable manifolds of the perturbed and unperturbed systems remain uniformly $\text{O}(\mu)$ close. This allows the Melnikov integral to be interpreted as the (normalized) distance between the stable and unstable manifolds at a specified point on the cross-section $\Sigma_0 = \{(X, p_X, \theta = \theta_0)\}$. Here, we do not have hyperbolic fixed points, but the results of McGehee [22], applied in Section 4.1, guarantee the existence of analytic stable and unstable manifolds. As in [8], we may therefore, apply the Hamiltonian reduction version of Melnikov's result ([16], Theorem 4.8.4):

Theorem 1. *Let $h^0 > 0$ and $I^0 = h^0/\Omega$. Let $\{H^X, H^1\}$ denote the Poisson bracket* [2] *of $H^X(X^0, p_X^0)$ and $H^1(X^0, p_X^0, \Omega t + \theta^0, I^0)$ evaluated along $X^0(t)$ and $p_X^0(t)$. Define the Melnikov function*

$$M(\theta_0) = \int_{-\infty}^{\infty} \{H^X, H^1\}(X^0, p_X^0, \Omega t + \theta^0, I^0)\,\mathrm{d}t \tag{4.23}$$

and assume that $M(\theta^0)$ has a simple zero. Then for $\mu > 0$ sufficiently small, the Hamiltonian system has transverse homoclinic orbits on the energy surface $H = h^0$.

---

[2] $\{F, G\} \overset{\text{def}}{=} \frac{\partial F}{\partial X}\frac{\partial G}{\partial p_X} - \frac{\partial F}{\partial p_X}\frac{\partial G}{\partial X}$

For the coupled system, there continue to exist orbits which start at $t = -\infty$ at the periodic orbit γ at $X = -\infty$ and which approach γ at $X = +\infty$ as $t \to +\infty$. By continuity, this must apply to the flow as well as to the Poincaré map. As a direct corollary to this, the system possesses *heteroclinic tangles* which direct the flow. The heteroclinic tangle will capture certain orbits and reflect or transmit them after allowing them to interact with the impurity mode a finite number of times. In addition, there exists a set of initial conditions of measure zero which start at $X = -\infty$ and are captured for all time. The heteroclinic tangle further implies the existence of chaotic motions in the dynamics.

To verify that the Melnikov function has simple zeros, we compute, using the expressions (4.7) and (4.8):

$$M(\theta_0) = \int_{-\infty}^{\infty} \left(\frac{\partial H^X}{\partial X} \frac{\partial H^1}{\partial p_X} - \frac{\partial H^X}{\partial p_X} \frac{\partial H^1}{\partial X} \right) dt = -\epsilon^2 \sqrt{\frac{2I^0}{\Omega}} \int_{-\infty}^{\infty} \cos\,(\Omega t + \theta_0)\, \mathrm{sech}^2 X (1 - 2\mathrm{sech}^2 X)\, dt.$$

Using the difference formula for cosines and the fact that, by choosing $t_1 = 0$ in Eq. (4.8), $\mathrm{sech}^2(X) = 2/(2+\epsilon t^2)$, we find

$$M = -2\epsilon^2 \sqrt{\frac{2I^0}{\Omega}} \cos \theta_0 \int_{-\infty}^{\infty} \cos \Omega t \frac{\epsilon t^2 - 2}{(\epsilon t^2 + 2)^2}\, dt. \tag{4.24}$$

It is clear that $M|_{\theta_0 = \pm \pi/2} = 0$ and $M'|_{\theta_0 = \pm \pi/2} \neq 0$, provided that the integral itself does not vanish. But the integral may be written as

$$\mathrm{Re} \int_{-\infty}^{\infty} \mathrm{e}^{\mathrm{i}\Omega t} \frac{\epsilon t^2 - 2}{(\epsilon t^2 + 2)^2}\, dt$$

and evaluated by residues by closing the contour in the upper half-plane to give

$$M = 2\pi \epsilon \sqrt{2I^0 \Omega} \cos \theta_0\, \mathrm{e}^{-\Omega \sqrt{2/\epsilon}}, \tag{4.25}$$

or, eliminating Ω in favor of ϵ, by Eq. (2.5):

$$M = 2\pi \sqrt{2I^0} G(\epsilon) \cos \theta_0, \tag{4.26}$$

where

$$G(\epsilon) \stackrel{\mathrm{def}}{=} \epsilon \left(1 - \tfrac{1}{4}\epsilon^2 \right)^{1/4} \mathrm{e}^{-\sqrt{2/\epsilon - \epsilon/2}}. \tag{4.27}$$

In Fig. 5, we plot $G(\epsilon)$, observing that it has no zeros for $\epsilon \in (0, 2)$, and exhibits a maximum at $\epsilon \approx 1.88$. We conclude that, for ϵ in the admissible range, the Melnikov function has simple zeros in θ_0 and hence, that $W^s(\gamma)$ intersects $W^u(\gamma)$ transversely. The maximum of $G(\epsilon)$ identifies the value of ϵ that gives greatest splitting distance between $W^s(\gamma)$ and $W^u(\gamma)$.

Fig. 6 illustrates the transverse intersections of the manifolds in the case $\mu = 0.5$, $\epsilon = 0.5$, $h^0 = 0.484$ (which corresponds to $I^0 = 0.5$). Here and in next sections, we use the $(X, Y = \dot{X})$ coordinates rather than the momentum variable p_X, but the pictures are equivalent via Eq. (4.2). Note that the stable and unstable manifolds intersect each other many times in these (relatively) short segments. Indeed, we may apply the Smale–Birkhoff theorem ([16], Theorem 5.3.5), modified as in [8], to conclude the existence of an invariant Cantor set of bounded motions on which the Poincaré map is topologically conjugate to a subshift of finite type: the system is chaotic.
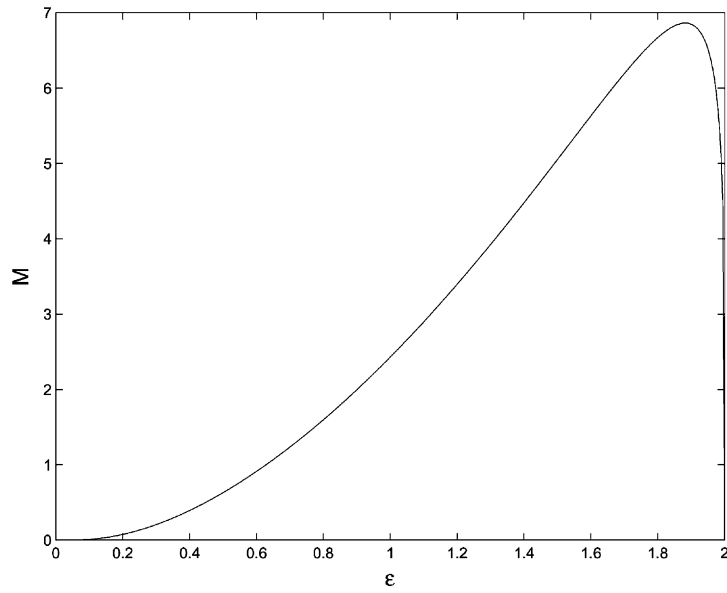
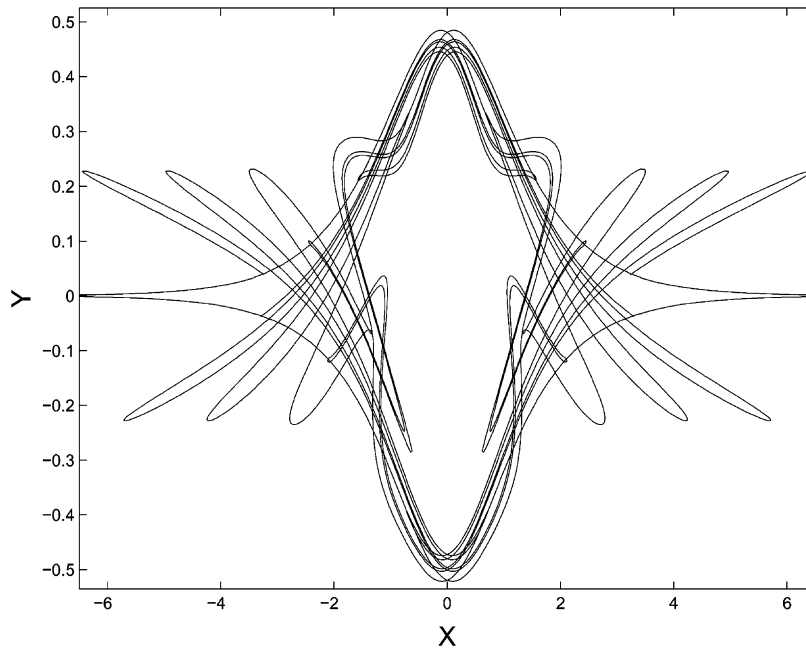Fig. 5. The nonvanishing factor, $G(\varepsilon)$, of the Melnikov function.

Fig. 6. The stable and unstable manifolds of the fixed points at $X = \pm\infty$ for the Poincaré map $P_{\pi/2}$, with parameters $\mu = 0.5$, $\epsilon = 0.5$, $I^0 = 0.5$.

4.3. Persistence of homoclinic orbits to $\mu = 1$

We may draw some useful implications from the symmetries (4.5a)–(4.5c), some of which are apparent in Fig. 6. Here we have plotted $W^{s,u}(X = \pm\infty)$ on the section $\Sigma_{\pi/2}$, corresponding to $a = 0$. Thus, via Eq. (4.5b), stable and unstable manifolds reflect into one another across the Y-axis. (Taking the section Σ_0 ($b = p_a = 0$), the reflection symmetry is about the X-axis.) This immediately implies that, if we can find a point ($X = 0, Y_0, a = 0, B_0, t = 0$) that lies in $W^s(X = +\infty)$ (respectively $W^s(X = -\infty)$), then this point also lies in $W^u(X = -\infty)$ (respectively $W^u(X = +\infty)$), and is therefore homoclinic to infinity (note the intersections on the Y-axis of Fig. 6). We note that this argument applies even in cases that Σ_{θ_0} fails to be a cross-section, which occurs for $\mu = O(1)$, depending on ϵ and μ. This failure is due to the fact that $\dot{\theta}$ changes sign, cf. remarks following Eq. (4.21). In this case we think of homoclinic orbits to the periodic orbit at infinity in the full flow, rather than the Poincaré map.

We now prove that homoclinic orbits to $|X| = \infty$ exist for all $\mu \leq 1$. In particular, consider arcs of initial conditions connecting the fixed point $(0, 0, 0, 0)$ to a point $(0, Y_0, 0, B_0)$. Orbits starting at or near $(0, 0, 0, 0)$ clearly remain trapped for all time; in fact no solution with energy $H = h_0 \in (-2\epsilon, 0)$ can escape to $|X| = \infty$, since its energy level lies below 0 and all trajectories satisfying $X(t) \to \infty$ satisfy $h_0 \geq 0$. In contrast, we prove in Appendix B that solutions starting at $(0, Y_0, 0, B_0)$ for sufficiently large $|Y_0|$ (depending on B_0) escape to $|X| = \infty$ with $|\dot{X} = Y| > 0$. Continuous dependence on initial data then implies that, on each arc connecting $(0, 0, 0, 0)$ to $(0, Y_0, 0, B_0)$, and in particular on arcs with $X = a = 0$, there is at least one orbit asymptotic to $(|X| = \infty, |Y| = 0)$. Hence, appealing to the symmetry Eq. (4.5b), we have a homoclinic orbit to infinity. However, this argument does not show that homoclinic orbits exist on *every* energy surface.

4.4. Phase space transport and lobe dynamics

Wiggins and coworkers [26,33] have developed a theory for transport of regions of phase space which is applicable to the map P_{θ_0} derived above. We summarize the relevant ideas, referring to Fig. 7, which shows part of the manifolds
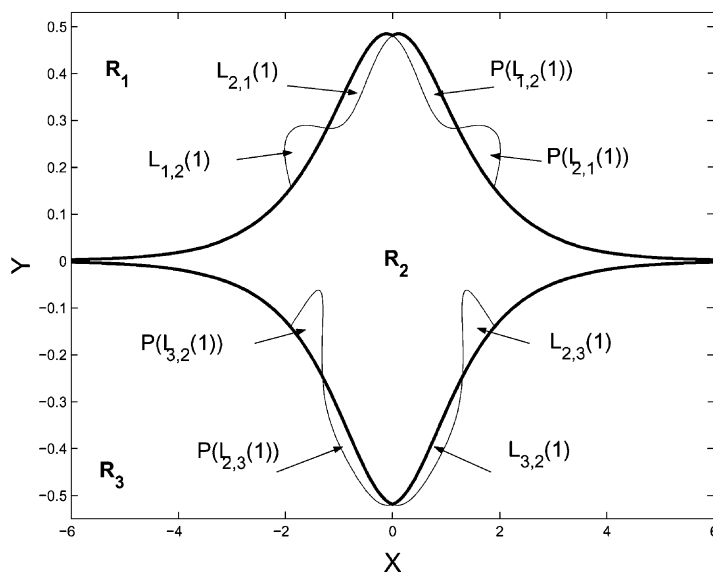

Fig. 7. The turnstiles governing phase space transport for the case $\mu = 0.5$, $\epsilon = 0.5$, $H = h_0 = 0.484$. $Y = \dot{X} = \frac{1}{8}p_X$.

$W^{s,u}(X = \pm\infty)$ for the Poincaré map $P_{\pi/2}$ (cf. Fig. 6). The bold portions of the manifolds, meeting at the *primary intersection points* q_i (here, on the symmetry axis $X = 0$), divide the section $\Sigma_{\pi/2}$ into three disjoint regions R_1, R_2, and R_3, analogous to those in the unperturbed phase plane of Fig. 6.

The images and preimages of q_i, $P_{\pi/2}^{\pm 1}(q_i)$ and the arcs of $W^{s,u}$ connecting them bound *lobes* that are mapped into one another by $P_{\pi/2}$ (recall that the lobe boundaries lie in invariant manifolds). In Fig. 7, we show the pairs of lobes forming the two *turnstiles* [21], along with their images. Specifically: the lobe $L_{i,j}(1)$ is the set of all points in region R_i which are mapped to region R_j under one iteration of P_{θ_0}. Note that $L_{i,j}(1) \subset R_i$ and $P_{\theta_0}(L_{i,j}(1)) \subset R_j$, and that points can only pass from R_i to R_j via the turnstile lobe $L_{i,j}(1)$. The turnstiles organize the capture dynamics of the map. In order for a rightward moving orbit to be captured, it must pass from R_1 to R_2. Hence, some image of its initial condition, $P_{\theta_0}^n(X_0, Y_0)$, must lie inside $L_{1,2}(1)$ for some $n > 0$; in other words, the point must be contained in a turnstile lobe preimage $P_{\theta_0}^{-n}(L_{1,2}(1))$. The first three such pre-images can be seen in the upper-left quadrant of Fig. 6. Similar observations apply to leftward moving orbits originating in R_3.

Consider the sequence of lobes in the upper right quadrant of Fig. 6. Here, sections of the unstable manifold of $X = -\infty$ form the boundaries of the lobes $P_{\theta_0}^k(L_{2,1}(1))$ for $k = 1, \ldots, 4$. Continuing the plot, we would find an infinite sequence of such lobes. The maxima (with respect to Y) of these lobes approach the horizontal asymptote $Y = \sqrt{H}/2 = \sqrt{h_0}/2$ and also approach equal spacing along that asymptote, since the flow of Eq. (2.11a) (and the reduced system (4.22)) approaches constant velocity away from the potential well at $X = 0$. This asymptote defines the maximum velocity with which kinks starting as trapped modes inside the well (with energy $\Omega I = h_0$) can escape, and thus, by symmetry across the Y axis, the maximum velocity for capture (this value can also be computed by solving for $\dot{X}$ as $X \to \infty$ with $I = 0$, given $H = h_0$).

Thus, far we have considered only those points that are trapped for at least one iterate. Once inside R_2 a point may subsequently enter a turnstile component $L_{2,j}(1)$, and then be ejected into R_1 or R_3. Moreover, since the images $P_{\theta_0}^k(L_{2,j}(1))$ all lie outside R_2, once ejected, orbits cannot re-enter, but must pass to $X = +\infty$ or $X = -\infty$. We now show that the probability of capture for all time is zero, and then analyze the topological structure and expected statistics of transient capture.

Proposition 1. *The set of points in $R_1 \cup R_3$ that is captured in R_2 and trapped for all future iterates, is of Lebesgue measure zero.*

Proof. Assume $D \subset R_1$ with meas$(D) > 0$, $P_{\theta_0}^N(D) \subset L_{1,2}(1)$, and $P_{\theta_0}^n(D) \subset R_2$ for all $n > N$, so that D is eventually trapped for all time (a similar argument applies to $D \subset R_3$). We claim that meas(R_2) is finite. This follows from the exponential decay of its boundaries $W^{u,s}(X = \pm\infty)$ as $|X| \to \infty$, since $W^{u,s}(X = \pm\infty)$ are close to the unperturbed separatrix (4.7) for large $|X|$. Now recall that P_{θ_0} preserves area. Then, since meas$(D) > 0$, $\sum_{n>N}$ meas$(P_{\theta_0}^n(D))$ must exceed meas(R_2), implying that there exists an integer $k \in [2, \infty)$ such that $P_{\theta_0}^{N+k}(D) \cap P_{\theta_0}^{N+1}(D) \equiv D_k$ is nonempty, and that its first preimage lies in R_2 (cf. the Poincaré recurrence Theorem). But, by hypothesis, $P_{\theta_0}^N(D) \subset L_{1,2}(1) \subset R_1$, and we have a contradiction. $\square$

In fact, the set of points trapped for all time has the local structure of the product of a Cantor set and an arc, and the gaps of the Cantor set correspond to orbits which are trapped for a finite number of iterates and then ejected. To understand this, it is helpful to consider an explicit and completely soluble example based on the standard Smale horseshoe [16,28]. Fig. 8 shows a map F defined on the unit square $S = [0, 1] \times [0, 1]$, with three hyperbolic saddle points at $(0, 0)$, $(0.5, 0.5)$ and $(1, 1)$. F is piecewise linear on the three horizontal strips H_i, $i = A, B, C$, whose images are the vertical strips $V_i = F(H_i)$. Indeed, we choose

$$DF|_{H_A \cup H_C} = \begin{bmatrix} \lambda_s & 0 \\ 0 & \lambda_u \end{bmatrix}, \qquad DF|_{H_B} = \begin{bmatrix} -\lambda_s & 0 \\ 0 & -\lambda_u \end{bmatrix}, \qquad \lambda_s < \frac{1}{3}, \lambda_u > 3. \tag{4.28}$$
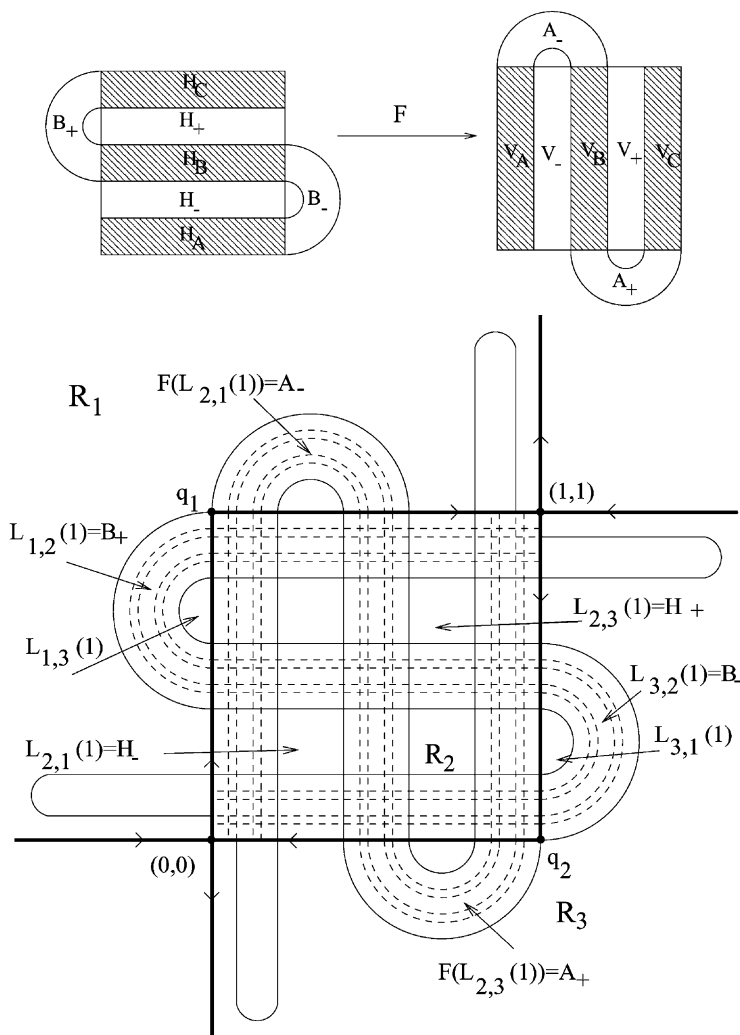
Fig. 8. A soluble trapping model.

The horizontal strips H_-, H_+ are mapped (nonlinearly) into the arches $A_\pm = F(H_\pm)$, and F is extended on the exterior of the unit square in the following manner. The preimages $F^{-1}(V_\pm)$ of the vertical strips $V_\pm$ are defined to be the arches $B_\pm$: thus, F acts nonlinearly on $B_\pm$ and the small semicircular regions 'inside' them, which are mapped 'inside' $A_\pm$; otherwise F is affine on the exterior of the square S, with $DF = DF|_{H_A \cup H_C}$. We indicate the action of F at the top of Fig. 8.

  The analogy with the mapping of Fig. 7 is as follows: the saddle points (1, 1) and (0, 0) correspond to the degenerate equilibria at $\pm\infty$, the invariant upper right and lower left quadrants 'outside' these points are neglected, and we focus on transport among regions R_1 (upper left), R_3 (lower right) and $R_2 = S$ (the unit square itself). The reader can check that the turnstile lobes $L_{1,2}(1) = B_+$, $L_{2,1}(1) = H_-$, $L_{3,2}(1) = B_-$ and $L_{2,3}(1) = H_+$ are as shown and that, in this case, there are also lobes $L_{1,3}(1)$ and $L_{3,1}(1)$, 'inside' $L_{1,2}(1)$ and $L_{3,2}(1)$, comprising

points that jump across R_2 in one iterate. Once inside $F(L_{2,1}(1)) = A_-$ or $F(L_{2,3}(1)) = A_+$, future iterates remain in R_1 or R_3 and march off to $\pm\infty$, as do preimages of points in $L_{3,2}(1)$ and $L_{1,2}(1)$.

We can explicitly compute the sets of points in $L_{i,2}(1) \cap F^{-k}(L_{2,j}(1))$; $i, j = 1, 3$, whose orbits are trapped for exactly k iterates before ejection back into R_1 or into R_3. First consider the sets $F^{-1}(H_\pm)$, which, since $H_\pm$ each contain three rectangles contained in V_i, are thin S-shaped strips crossing H_A, H_B and H_C and connecting them via thin arches inside $L_{3,2}(1)$ and $L_{1,2}(1)$. Thus the four components of $L_{i,2}(1) \cap F^{-1}(L_{2,j}(1))$; $i, j = 1, 3$ are semicircular arches, two each inside $L_{1,2}(1)$ and $L_{3,2}(1)$. For $k > 1$ we must compute further preimages $F^{-k}(H_\pm)$, but, since F is piecewise linear on sets that remain in $R_2 = S$, each component of this is a horizontal strip contained in H_A, H_B, or H_C. Taking a further preimage of any single component, one finds a thinner arch inside $L_{3,2}(1)$ or $L_{1,2}(1)$, and $L_{i,2}(1) \cap F^{-2}(L_{2,j}(1))$ consists of two thinner arches lying in each of the three components of $L_{i,2}(1) \backslash F^{-1}(L_{2,j}(1))$. The sets $L_{i,2}(1) \cap F^{-k}(L_{2,j}(1))$; $i, j = 1, 3$, therefore, each comprise 2×3^k arches, which are the gaps in the iterative construction of a Cantor set of *arcs* which belong to $W^s(0, 0)$ and $W^s(1, 1)$, and comprise the points which are trapped for all time.

The widths of the gap-arches, and hence the probabilities of trapping, are determined by the expansion eigenvalue λ_u. Assuming symmetry, the heights of $H_\pm$ are $\alpha \overset{\text{def}}{=} (\lambda_u - 3)/2\lambda_u$, since each strip H_i is stretched by a factor λ_u to achieve height 1. Again assuming uniformity in the nonlinear portions of F, we may compute the desired widths from the gap widths in a Cantor set in which *two* gaps of width α, symmetrically placed, are removed from each remaining closed interval at each step. Starting with a unit interval, we compute the lengths $L(k)$ removed at each step, obtaining

$$L(k) = 2\alpha(1 - 2\alpha)^{k-1} = \frac{\lambda_u - 3}{\lambda_u} \left(\frac{3}{\lambda_u}\right)^{k-1}. \tag{4.29}$$

Note that $\sum_{k=1}^{\infty} L(k) = 1$: as we expect from Proposition 1, the Cantor set itself is of measure zero. Moreover, plotting $L(k)$ versus k, we obtain the distribution of residence times for trapped orbits as an exponentially decaying curve. We test this prediction for the model at hand in Section 5.

5. The Poincaré maps

To test the predictions of the transport theory outlined above, we performed the following numerical experiments. We seeded the turnstile lobe $L_{1,2}(1)$ with 5000 points, computed their orbits under $P_{\pi/2}$ until they left R_2, and plotted a histogram of residence times (number of iterates spent in R_2). We used the same parameter values as in Fig. 6. Fig. 9 clearly indicates exponential decay, with an exponent -0.038 (the least squares fit is also shown). Approximately two-thirds (65%) of the orbits pass to R_3 and are reflected to $X = -\infty$ and one-third return to R_1 and are transmitted to $X = +\infty$.

To investigate the topological structure of the lobe intersections, we took 100 initial conditions along a line crossing $L_{1,2}(1)$ approximately parallel to $W^u(X = -\infty)$ and recorded an integer k equal to the number of iterates the orbit remained in R_2, positive integers indicating transmission to R_1 and negative, reflection to R_3. The resulting bar graph is shown in Fig. 10. Focusing on the largest 'gaps', we note a central set of points with $k = 9$, and two flanking sets with $k = -3$. In general, as for the soluble model of Fig. 8, as gap sizes decrease, residence times increase.

We note that the turnstile lobes of the stable and unstable manifolds of Figs. 6 and 7 do not 'intersect cleanly', as in the case of Fig. 8 analyzed above: only on and after the *third* iterate does $F^k(L_{1,2}(1))$ intersect $W^u(X = +\infty)$. It is this 'incompleteness' that leads to the imbalance of points ejected into R_1 and R_3: the preimages of $L_{2,1}(1)$ and $L_{2,3}(1)$ intersecting $L_{1,2}(1)$ are not of equal areas.
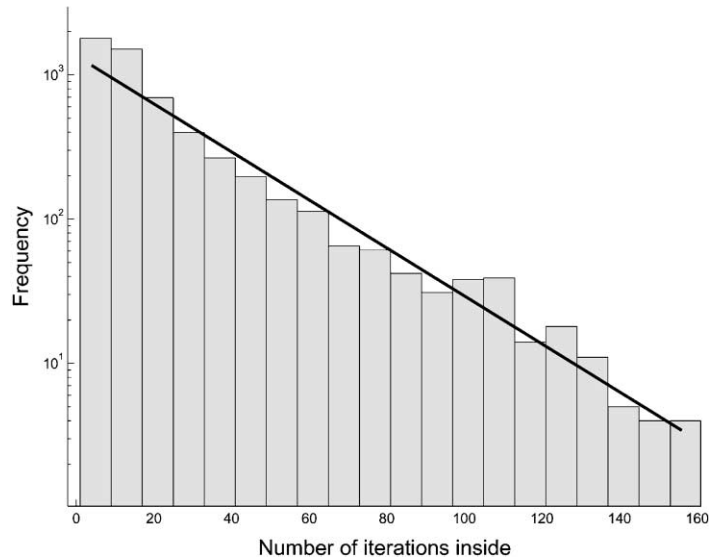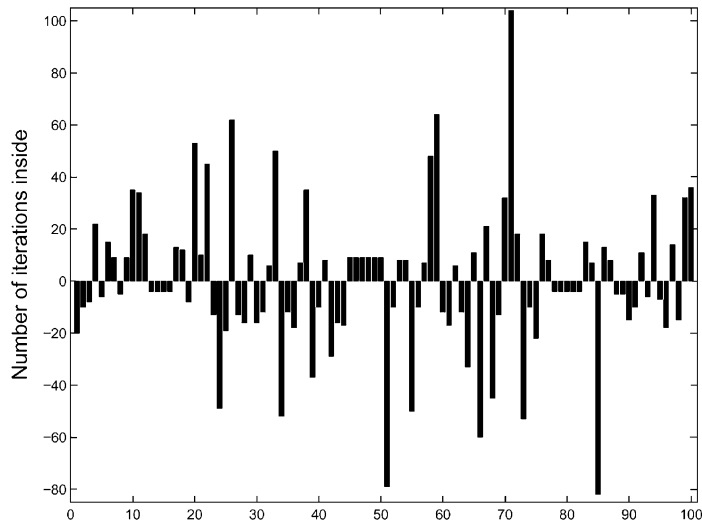
Fig. 9. A histogram of residence times in R_2.

Fig. 10. Evidence for the Cantor set lobe substructure.

6. Coupling to radiation

The system Eq. (2.1) is a dispersive nonlinear partial differential equation whose solutions are composed of a combination of coherent structures (kinks, defect modes) and dispersive waves. In the model, Eqs. (2.11a) and (2.11b), we have replaced the infinite dimensional system by a finite dimensional system for the "collective coordinates" $X(t)$ and $a(t)$ describing the kink location and defect mode amplitude. The system, Eqs. (2.11a) and (2.11b), is energy conserving, being derived from an effective Lagrangian, Eq. (2.8), which is an approximate finite

dimensional reduction of the full Lagrangian, Eq. (2.8). This reduction neglects nonlinear coupling to radiation modes, an infinite dimensional subspace. Such coupling will result in energy exchange between the coherent structures and the radiation modes. The net effect of coupling to radiation modes appears to be that the subsystem, approximately governed by Eqs. (2.11a) and (2.11b), experiences dissipation; some of the energy of the kink-defect mode system is carried off to spatial infinity. This enhances the defect's capacity for trapping the kink, in a manner analogous to the opening of basins of attraction in the undamped pendulum phase portrait, upon inclusion of dissipative friction.

A rigorous derivation of the (radiation-induced) dissipative correction to a finite dimensional collective coordinate equation and infinite time analysis of the full system was implemented in a simpler but closely related problem in [29]. In the present language, the problem considered there concerned the nonlinear interaction between a single defect mode and radiation modes for solutions of small norm. To see how we arrive at this correction, we rewrite Eq. (2.1) as

$$u_{tt} - u_{xx} + u - \epsilon\delta(x)u = g(u, x), \tag{6.1}$$

where $g(u, x) = [1 - \epsilon\delta(x)](u - \sin u)$. Consider Eq. (6.1) with small amplitude initial data, which decays to zero as $|x| \to \infty$. Since $u - \sin(u)$ is cubic in u for small u, Eq. (6.1) can be viewed as a nonlinear perturbation of a linear wave equation with a single bound state. This is essentially the question addressed in [29].[3] For small amplitude initial conditions it is natural to decompose $u(x, t)$ into the bound state and continuous spectral components associated with the linear problem (2.3) obtained by setting $g = 0$. Thus, we let

$$u(x, t) = a(t)\varphi(x) + \eta(x, t), \quad \langle \varphi, \eta(\cdot, t) \rangle = 0, \tag{6.2}$$

where φ denotes the normalized defect mode. Substitution of Eqs. (6.1) and (6.2) and projecting onto the defect mode and its orthogonal complement (the radiation modes) yields a coupled system for $a(t)$ and $\eta(x, t)$. It is natural to think of solving for $\eta(\cdot, t)$ as a functional of $a(t)$ and then substituting the result into the equation for $a(t)$ to get a closed equation for $a(t)$, in which the radiative effects are taken into account. This scheme, in the spirit of a center manifold reduction, can be implemented to high enough order to make explicit the radiation-induced dissipation. η solves a nonlinear wave equation with a forcing term proportional to $a^3(t)\varphi^3(x)$, which contains the time-frequency 3Ω. Since continuum frequencies, Ω, satisfy $\omega^2 > 1$, if the third harmonic lies in the continuous spectrum ($3\Omega > 1$, corresponding here to $0 < \epsilon < 4\sqrt{2}/3$), then this contribution to the forcing resonates with continuum modes. A careful calculation of the effect of this resonance [29] leads, after a near-identity change of variables, to a *damped* oscillator of the following type,

$$\ddot{a} + \left(\Omega^2 + O(|a|^2)\right)a = -\Gamma a^4 \dot{a}, \tag{6.3}$$

where Γ is generically strictly positive. This is the key to showing that the defect mode, a spatially localized and time-periodic state for the linear limiting equation, does not persist for the nonlinear problem, but is rather *metastable* and slowly decays to zero.

In the current problem, the solution u is a spatially localized perturbation of the kink (rather than of the zero solution). Thus, in place of Eq. (2.6), we set

$$u = u_k + u_{im} + \eta(t, x), \tag{6.4}$$

where $\eta(t, x)$ denotes the part of the solution consisting of dispersive waves. The same mechanisms described above are expected to be at work. Formal calculations [31] indicate that the simplest coupling to radiation modes occurs

---

[3] The main differences are that in [29], the wave equation considered was in three space dimensions; $\epsilon\delta(x)$ is replaced by a smooth potential with one bound state, and $g(u, x) \sim u^3$, with no explicit spatial dependence. The methods of [29] can be adapted to the current situation.
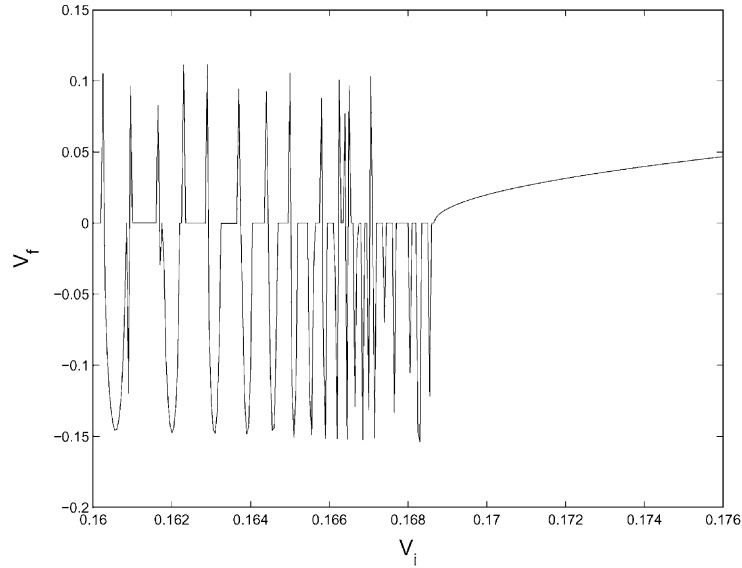
Fig. 11. Output velocity V_f vs. input velocity V_i in the presence of radiation induced damping, with $\epsilon = 0.5$, $\Gamma = 16$. The behavior is simplified in comparison with Fig. 3: below critical velocity, solutions may be captured, reflected, or transmitted, but the sensitivity to initial conditions is decreased. For smaller values of Γ, more reflection and transmission bands survive.

if the second harmonic lies in the continuous spectrum ($2\Omega > 1$ or $\epsilon < \sqrt{3}$). Formal inclusion of the damping correction arising from this resonance in the system Eqs. (2.11a) and (2.11b) yields a reduced system of the form

$$8\ddot{X} + U'(X) + aF'(X) = 0 \tag{6.5a}$$

$$\ddot{a} + \Omega^2 a + \tfrac{1}{2}\epsilon F(X) = -\epsilon^3 \Gamma F(X)^2 a^2 \dot{a} \tag{6.5b}$$

where $\Gamma > 0$.

In Fig. 11, we show the analog of Fig. 2 with the nonlinear damping of Eq. (6.5b) active with $\epsilon = 0.5$ and $\Gamma = 16$. In the presence of damping, the output velocity is a much less sensitively dependent function of the input velocity than in the case without damping. In this case, below the critical velocity v_c, many trajectories are captured, except for a few intervals, most of which lead to reflection, as in Fig. 2. The incorporation of radiation damping effects present in the full dynamical system "smoothes out" the dynamics; many reflection resonance bands and most transmission bands appear to be eliminated. For smaller Γ values, more reflection and transmission bands survive, while for higher Γ, fewer transmission bands survive.

The Hamiltonian reduction of Section 4.2 can no longer be used directly, since the damping term of Eq. (6.5b) leads to decay of H, and an evolution equation for H must be added to the reduced system Eq. (4.22) (the flow of Eqs. (6.5a) and (6.5b) is volume-contracting, and the fixed point at the origin becomes a (degenerate) sink). However, much as in [17], Section 5, we may conclude that "ghost horseshoes" persist for small Γ. In particular, since $|F(X)| \to 0$ as $|X| \to \infty$, all the degenerate periodic orbits γ_{h_0} at infinity survive, along with their stable and unstable manifolds $W^{s,u}(\gamma_{h_0})$. The unions of such manifolds $\mathcal{U}^{s,u} = \cup_{h_0 \in (0, h_{max})} W^{s,u}(\gamma_{h_0})$ are three-dimensional. One may now define a three-dimensional cross section $\Sigma' = \{(X, p_X, H, \theta = \theta_0)\}$ and conclude that $\mathcal{U}^{s,u}$ intersect Σ' in two-dimensional surfaces: essentially, one has a stack of copies of Fig. 6. The Melnikov computation and arguments of Section 4.3 guarantee that, for small $\Gamma \ll \mu$, these surfaces still intersect transversally, although orbits of the Poincaré map now lose energy, and hence move in the direction of decreasing H. In particular, three-dimensional analogs of the lobes

and turnstiles of Fig. 7 persist, albeit they are now "invaded" by the stable manifold of the origin. Orbits exhibiting transient chaos and escape via transmission or reflection (with $H \to$ constant as $|X| \to \infty$) persist, but now the set of captured orbits has strictly positive measure, since the flow is volume-contracting.

7. Discussion and conclusions

In this study, we have examined a model of kink-defect interactions in the sine-Gordon equation. We use the model's Hamiltonian structure to give a rather complete characterization of the dynamics. We demonstrate that a soliton propagating toward a defect may oscillate around the defect any integer number of times before being ejected, either in the original direction or in the opposite direction, and propagating off to infinity, leaving some of its energy in the stationary defect mode. This behavior is governed by phase-space transport in the *Poincaré map* of the system, which exhibits sensitive dependence on initial conditions and chaotic behavior. The initial conditions leading to differing behaviors are intricately interwoven. It also shows that capture of kinks for all positive times can only occur for measure-zero sets of initial conditions. A comparison is made with a horseshoe map, for which a complete description of the behavior is given, and we show numerically that the dynamics show similar statistical behavior to those of the horseshoe map.

This contrasts strongly with numerical simulations of the full sine-Gordon equations [11], and with our own numerical results on equations Eqs. (6.5a) and (6.5b) in the presence of a damping term. In both of these cases, the dynamics is much simpler. The strong interlacing of behavior regimes is replaced by a simpler condition: kinks moving above a critical velocity escape, those below that velocity are captured, except in a few resonance bands, where kinks are reflected. Two questions of interest are the following: (1) Can one obtain a more detailed understanding of how the addition of dissipation alters the Hamiltonian dynamics than that sketched at the end of Section 6? (2) Can an effective dissipation law due to nonlinear resonant coupling to radiation be rigorously derived?

The study of capture orbits in Hamiltonian dynamical systems has its origins in celestial mechanics. The general problem is as follows: do there exist collisionless solutions to the n-body problem for which the interparticle distances are bounded for all positive times, but for which some or all of the interparticle distances diverge as $t \to -\infty$. Littlewood [20] proved that such a set has measure zero (cf. Siegel and Moser [27], Section 37). More precisely ([20], Theorem 2), almost all points in the set of collisionless solutions bounded as $t \to +\infty$ also belong to the set of solutions bounded as $t \to -\infty$. Specific examples of such solutions for the three-body problem, with suitable restrictions on the masses, are described by Alekseev [1]. As in the problem we study, a variation on the Poincaré recurrence theorem shows that capture orbits occupy a set of measure zero.

A generalization of interest is when the defect is not a δ-function, but of nonzero spatial extent. We have studied this question in the context of gap soliton capture in the nonlinear coupled mode equations (NLCME) [14]. In detailed numerical experiments, we find many possible interactions between the pulse and the defect mode, including reflection, transmission, capture, and additional regimes where the pulse is destroyed by its interaction with the defect. Capture depends on resonance between the incoming gap soliton and an energetically accessible *nonlinear defect mode* "pinned" at the defect. We are currently investigating a similar mechanism for nonlinear Schrödinger equations, and its connection with finite dimensional models of the type studies here.

Diacu for drawing our attention to Littlewood's paper, and our editor Chris Jones and one of the referees for pointing out the work of Birnir and Campbell et al.

Appendix A. McGehee's stable manifold theorem

For completeness, we state the stable manifold theorem for degenerate maps proved in [22], Theorem 1. Let $B(\beta, \delta)$ denote the sector centered on the positive ξ-axis:

$$B(\beta, \delta) = \{(\xi, \eta) \in R^2 : 0 \le \xi \le \delta, |\eta| \le \beta\xi\},$$

and $A^+(f, B)$ denote the positively invariant set (=stable manifold) restricted to B:

$$A^+(f, B) = \{(\xi, \eta) \in B : f^k(\xi, \eta) \in B \quad \forall k > 0, \quad f^k(\xi, \eta) \to (0, 0), \text{ as } k \to \infty\}.$$

Theorem 2. *Let* $f: R^2 \to R^2$ *be real analytic and of the form*

$$f := id + p + r,$$ (A.1)

where id *is the identity,* $p = (p_1, p_2)$ *is a homogeneous polynomial of degree* $n \ge 2$, *and* r *consists of terms of degree at least* $n + 1$. *Suppose further that, for* $\xi > 0$:

$$p_1(\xi, 0) < 0, \quad p_2(\xi, 0) = 0, \quad \frac{\partial p_2}{\partial \eta}(\xi, 0) > 0.$$ (A.2)

Then there exist positive constants β *and* δ *such that* $A^+(f, B)$ *is the graph of a differentiable function* $\phi : [0, \delta] \mapsto R^1$. *Furthermore* $\phi|_{(0,\delta]}$ *is real analytic.*

The unstable manifold is treated by considering the inverse map f^{-1}.

Appendix B. Proof of claim of Section 4.3

The proof proceeds in two steps. First we examine the direction of the vector field of Eqs. (4.1a) and (4.1b) through a certain hypersurface in the phase space. We then show that trajectories with sufficiently large initial kink velocity $Y_0 = p_X(0)/8$ cannot cross this hypersurface, which gives a lower bound on the velocity of the kink.

Let

$$\mathcal{F} = -4\sqrt{2\epsilon} \operatorname{sech} X + p_X - \sqrt{2\epsilon}C,$$ (B.1)

so that $\mathcal{F} = 0$ defines a hypersurface $\mathcal{M}$ in the four-dimensional phase space at a distance C above the separatrix from the uncoupled ($\mu = 0$) system. A trajectory of Eqs. (4.1a) and (4.1b) starting above $\mathcal{M}$ cannot cross $\mathcal{M}$ at points where the vector field points upward through $\mathcal{M}$, i.e. where

$$\nabla\mathcal{F} \cdot \vec{v}|_{\mathcal{F}=0} \ge 0,$$ (B.2)

where $\vec{v}$ is the Hamiltonian vector field defined by Eqs. (4.19a)–(4.19d). The inner product is given by

$$\nabla\mathcal{F} \cdot \vec{v} = 4\sqrt{2\epsilon} \operatorname{sech} X \tanh X \cdot \tfrac{1}{8} p_X|_{p_X=\sqrt{2\epsilon}(C+4\operatorname{sech} X)} - U'(X) - \mu a F'(X)$$

$$= 2\epsilon \operatorname{sech} X \left(\frac{C}{2} \tanh X - \mu a(1 - 2\operatorname{sech}^2 X) \right).$$ (B.3)

We may show that this is positive if and only if

$$e^{2X}\left(\tfrac{1}{2}C - \mu a\right) - e^{-2X}\left(\tfrac{1}{2}C + \mu a\right) + 6\mu a > 0. \tag{B.4}$$

We consider the evolution of Eqs. (4.1a) and (4.1b) with initial conditions

$$(X, p_X, a, p_a) = (0, p_X(0), 0, p_a(0)) \tag{B.5}$$

and show that for $p_X(0)$ sufficiently large, the trajectory cannot cross $\mathcal{M}$. First we bound the growth rate of I and use this to give lower bounds for p_X and X for (small) finite times. We bound I using Eq. (4.19c) and the fact that $|\sin\theta F(X) \leq 1$,

$$\sqrt{I(t)} \leq \sqrt{I(0)} + \epsilon\mu\sqrt{\frac{\epsilon}{\Omega}}t. \tag{B.6}$$

Using this bound on $\sqrt{I}$, then for fixed T and $0 \leq t \leq T$

$$p_X(t) \geq p_X^* = p_X(0) - 2\epsilon\left(\left(2 + \mu\sqrt{\frac{\epsilon I(0)}{\mu}}\right)T + \frac{\epsilon^2\mu^2}{2\Omega}T^2\right), \tag{B.7}$$

and p_X^* can be made as large as we need by suitable choice of $p_X(0)$. It follows from Eq. (4.19a) that

$$X(t) \geq \tfrac{1}{8}p_X^* t. \tag{B.8}$$

Therefore, by choosing $p_X(0)$ sufficiently large, we may force the dynamics to evolve such that $X(T)$ reaches any chosen value of $X^* > 0$. In particular, we may assume that $X(T)$ reaches the value $X = 1$ while $p_X > p_X^*$ remains strictly positive. We may thus restrict our attention to the direction of $\vec{v}$ along $\mathcal{M}$ in the region $X \geq 1$. From Eq. (B.4), we determine that the vector field points upward through $\mathcal{M}$ as long as

$$C > \frac{2}{1 - e^{-4}}\mu a \overset{\text{def}}{=} B\mu a. \tag{B.9}$$

We now use the bounds on p_X and X to give better control of I and hence a. As long as $p_X > 0$, we may use the relation

$$\frac{d}{dt} = \frac{p_X}{8}\frac{d}{dX}$$

to write the evolution equation for I as

$$\frac{p_X}{8}\frac{dI}{dX} = \mu\sqrt{\frac{I\epsilon}{\Omega}}\sin\theta F(x) \tag{B.10}$$

so that

$$\sqrt{I(t)} \leq \sqrt{I(0)} + 4\mu\sqrt{\frac{\epsilon}{\Omega}}\int_0^X \frac{|F(X)|}{p_X}\,dX. \tag{B.11}$$

As long as $p_X \geq p_X^*$, using $F(X) = -2\epsilon\,\text{sech}\,X\,\tanh X$, this gives

$$\sqrt{I(t)} \leq \sqrt{I(0)} + \frac{8\mu\epsilon}{p_X^*}\sqrt{\frac{\epsilon}{\Omega}}. \tag{B.12}$$

With all these pieces we may now prove the claim. Given $C > 0$, $\epsilon \in (0, 2)$, $\mu \in (0, 1)$, and T, choose $p_X(0)$ such that

$$p_X(t) \geq p_X^* \geq \sqrt{2\epsilon}(C + 4\text{sech}\,1) > 0 \quad \forall t \in [0, T] \tag{B.13}$$

and $\quad X(T) \geq \frac{1}{8} p_X^* T \geq 1.$ (B.14)

Therefore, the trajectory lies above $\mathcal{M}$ in the phase space at $X = 1$. We claim that the above choices of $C > 0$ and $p_X(0)$ may be made such that

$$\dot{X} = \frac{1}{8} p_X \geq \frac{1}{8} \sqrt{2\epsilon}(C + 4\,\text{sech}\,X) \geq \frac{1}{8} \sqrt{2\epsilon}C$$

and hence, the solution escapes to $+\infty$.

Supposes that this fails, and the trajectory crosses $\mathcal{M}$ at $X = X_1 > 1$, then X continues to increase until this time and

$$p_X \geq \sqrt{2\epsilon}(C + 4\,\text{sech}\,X) \geq \sqrt{2\epsilon}C,$$

so that, by Eq. (B.12),

$$\sqrt{I(t)} \leq \sqrt{I(0)} + \frac{8\mu\epsilon}{\sqrt{2\epsilon}C}\sqrt{\frac{\epsilon}{\Omega}}$$

and, by Eq. (4.15)

$$a \leq \sqrt{\frac{\epsilon I(0)}{\Omega}} + \frac{8\mu\epsilon^2}{\sqrt{2\epsilon}\Omega C}.$$ (B.15)

Because, by inequality Eq. (B.9), a trajectory cannot cross $\mathcal{M}$ when $C > B\mu a$, at the crossing, we must have $C \leq B\mu a$. Combining this with Eq. (B.15) yields

$$C \leq B\mu \left(\sqrt{\frac{\epsilon I(0)}{\Omega}} + \frac{8\mu\epsilon^2}{\sqrt{2\epsilon}\Omega C} \right) \Rightarrow C^2 \leq B\mu \left(\sqrt{\frac{\epsilon I(0)}{\Omega}}C + \frac{8\mu\epsilon^2}{\sqrt{2\epsilon}\Omega} \right).$$ (B.16)

If C and $p_X(0)$ are chosen sufficiently large, however, inequality Eq. (B.16) cannot hold, and we have a contradiction. Therefore, given $p_a(0)$ (i.e. given $I(0)$), it is possible to choose $p_X(0)$ sufficiently large such that for initial conditions $(0, p_X(0), 0, p_a(0))$, the solution escapes to infinity at a nonzero rate.

References

[1] V.M. Alekseev, On the possibility of capture in the three-body problem with a negative value for the total energy constant, Uspehi Mater. Nauk 24 (1969) 185–186.

[2] B. Birnir, Chaotic perturbations of KdV equations. I. Rational solutions, Physica D 18 (1986) 464–466.

[3] B. Birnir, Chaotic perturbations of KdV: Rational solutions, Physica D 19 (1986) 238–254.

[4] D.K. Campbell, M. Peyrard, Kink–antikink interactions in the double sine-Gordon equation, Physica D 19 (1986) 165–205.

[5] D.K. Campbell, M. Peyrard, Solitary wave collisions revisited, Physica D 18 (1986) 47–53.

[6] D.K. Campbell, J.S. Schonfeld, C.A. Wingate, Resonance structure in kink–antikink interactions in ϕ^4 theory, Physica D 9 (1983) 1–32.

[7] X.D. Cao, B.A. Malomed, Soliton-defect collisions in the nonlinear Schrödinger equation, Phys. Lett. A 206 (1995) 177–182.

[8] H. Dankowicz, P. Holmes, The existence of transverse homoclinic points in the Sitnikov problem, J. Diff. Equat. 116 (1995) 468–483.

[9] C.M. de Sterke, J.E. Sipe, Envelope-function approach for the electrodynamics of nonlinear periodic structures, Phys. Rev. A 38 (1988) 5149–5165.

[10] Z. Fei, Y.S. Kivshar, L. Vázquez, Resonant kink-impurity interactions in the ϕ^4 model, Phys. Rev. A 46 (1992) 5214–5220.

[11] Z. Fei, Y.S. Kivshar, L. Vázquez, Resonant kink-impurity interactions in the sine-Gordon model, Phys. Rev. A 45 (1992) 6019–6030.

[12] K. Forinash, M. Peyrard, B. Malomed, Interaction of discrete breathers with impurity modes, Phys. Rev. E 49 (1994) 3400–3411.

[13] H. Goldstein, Classical Mechanics, 2nd Edition, Addison-Wesley Series in Physics, Addison-Wesley Publishing Co., Reading, MA, 1980.

[14] R.H. Goodman, R.E. Slusher, M.I. Weinstein, Stopping light on a defect, J. Opt. Soc. Am. B, 2001 (submitted for publication).

[15] R.H. Goodman, M.I. Weinstein, P.J. Holmes, Nonlinear propagation of light in one-dimensional periodic structures, J. Nonlinear Sci. 11 (2001) 123–168.

[16] J. Guckenheimer, P. Holmes, Nonlinear Oscillations, Dynamical Systems, and Bifurcations of Vector Fields, Springer-Verlag, New York, 1983.

[17] P. Holmes, J.E. Marsden, Horseshoes in perturbations of Hamiltonian systems with two degrees of freedom, Commun. Math. Phys. 82 (1982) 523–544.

[18] Y. Kivshar, private communication.

[19] Y.S. Kivshar, Z. Fei, L. Vázquez, Resonant soliton-impurity interactions, Phys. Rev. Lett. 67 (1991) 1177–1180.

[20] J.E. Littlewood, On the problem of n bodies, Comm. Sém. Math. Unvi. Lund [Medd. Lunds Univ. Mat. Sem.], Tome Supplémentaire, 1952 (1952) 143–151.

[21] R. MacKay, J. Meiss, I. Percival, Transport in Hamiltonian systems, Physica D 13 (1984) 55–81.

[22] R. McGehee, A stable manifold theorem for degenerate fixed points with applications to celestial mechanics, J. Diff. Equat. 14 (1973) 70–88.

[23] D.W. McLaughlin, A.C. Scott, Perturbation analysis of fluxon dynamics, Phys. Rev. A 18 (1978) 1652–1680.

[24] V.K. Melnikov, On the stability of the center for time periodic perturbations, Trans. Moscow Math. Soc. 12 (1963) 1.

[25] M. Peyrard, D.K. Campbell, Kink–antikink interactions in a modified sine-Gordon model, Physica D 9 (1983) 33–51.

[26] V. Rom-Kedar, S. Wiggins, Transport in two-dimensional maps, Arch. Rational Mech. Anal. 109 (1990) 239–298.

[27] C.L. Siegel, J.K. Moser, Lectures on Celestial Mechanics, in: C.I. Kalme (Ed.), Die Grundlehren der mathematischen Wissenschaften, Band 187, Springer-Verlag, New York, 1971.

[28] S. Smale, Differentiable dynamical systems, Bull. Am. Math. Soc. 73 (1967) 747–817.

[29] A. Soffer, M.I. Weinstein, Resonances and radiation damping in Hamiltonian nonlinear wave equations, Invent. Math. 136 (1999) 9–74.

[30] D.M.A. Stuart, Perturbation theory of kinks, Commun. Math. Phys. 149 (1992) 433–462.

[31] M.I. Weinstein, unpublished note.

[32] M.I. Weinstein, Modulational stability of ground states of nonlinear Schrödinger equations, SIAM J. Math. Anal. 16 (3) (1985) 472–491.

[33] S. Wiggins, Chaotic Transport in Dynamical Systems, Springer-Verlag, New York, 1992.